Kovove Mater. 51 2013 333–341
DOI: 10.4149/km_2013_6_333

The performance of TV-MOPSO in optimization of sintered steels

A. Mazahery, M. Ostad Shabani*

Karaj Branch, Islamic Azad University, Karaj, Iran

Received 27 April 2012, received in revised form 26 September 2012, accepted 25 November 2012

Abstract

During the last decade novel computational methods have been introduced in some fields of engineering sciences. In this article, we describe a novel Particle Swarm Optimization (PSO) approach to multi-objective optimization, called Time Variant Multi-Objective Particle Swarm Optimization (TV-MOPSO). The mechanical and tribological behaviors of sintered steel have been experimentally investigated. TV-MOPSO is made adaptive in nature by allowing its vital parameters to change with iterations. This adaptiveness helps the algorithm to explore the search space more efficiently. A new diversity parameter has been used to ensure sufficient diversity amongst the solutions of the non-dominated fronts, while retaining at the same time the convergence to the Pareto-optimal front.

K e y w o r d s: wear, steel, swarm

1. Introduction

Over the past quarter century, there has been an upsurge in popularity of manufacturing machine components through Powder Metallurgy (PM) among all other processes, which is the outcome of its capability for near-net shape forming, as well as relatively low energy consumption and manufacturing cost [1–5]. These products possess excellent structural homogeneity and fine microstructure which is quite impossible to be obtained by conventional casting processes [6–8]. Powder metallurgy process generally consists of four basic steps: (1) powder manufacture, (2) powder mixing and blending, (3) compacting, (4) sintering. Compacting is generally performed at room temperature, and the elevated-temperature process of sintering is usually conducted at atmospheric pressure [9–13].

Pre-alloying is a special powder metallurgy term for the production of alloyed powders usually from a melt by water or gas atomization. The melt typically exhibits the same composition as the emerging powder particles. Alloying elements are uniformly distributed in the solid solution in the all pre-alloyed powder particles or are present at the separate phases in high alloy powders. In pre-alloyed powders used for production of structural steels, the first case applies. Generally, the alloy elements that do not strongly affect the compressibility of the powders, e.g., Mo and Cr, are introduced through the pre-alloy route while those that result in strong solid strengthening such as Ni, Cu, and Mn are either admixed or diffusion bonded [2, 4, 6]. The use of diffusion alloyed steel powders is an intuitive approach to solve the problems associated with powder metal products including inhomogeneous microstructure, inadequate dimensional control and mechanical properties. Diffusion alloyed steel powders augment the possibility for preparation of new varieties in production of PM parts with high mechanical and some special properties. Typical commercial systems are Fe-1.5Mo + 2 % Ni, Fe-1.5Mo + 2 % Cu, and Fe-1.5Mo + 4 % Ni + 2 % Cu which are available as diffusion bonded grades.

The combination of relatively high levels of copper, nickel, and molybdenum provides a cost-effective alloy, but with sufficient alloy content to provide the desired microstructure with the required hardness and wear resistance. Currently, the mainstream PM alloy system used for such applications mentioned above is the series, containing iron with chromium and nickel additions. Because of frequent direct contact of these components during their work cycles, studying the wear behavior of sintered steels is of great importance. It is reported that the oxidation wear, abrasive wear and delamination are the major wear mechanisms in these

*Corresponding author: tel.: +98 912 563 6709; fax: +98 261 6201888; e-mail address: vahid_ostadshabany@yahoo.com

sintered steels. Meanwhile, depending on the shape of pores and microstructure of materials as well as conditions of wear test such as applied load, the amount of porosity can be beneficial or detrimental to wear resistance [5–8, 14–20].

Furthermore, during the last decade novel computational methods have been introduced in some fields of engineering sciences. Particle swarm optimization, which was originally proposed by Kennedy in 1995, is a relatively new and robust optimization technique. It has attracted great attention due to the simplicity and efficiency in recent years. Similar to genetic algorithm, PSO is a population-based random search technique and it is easy to use since the algorithm requires fewer parameters. At present, PSO has been applied extensively to various fields, such as function optimization, filter design, proportional-integral-derivative control, power allocation, biological information extraction, and other scientific and engineering problems [21–27]. However, van den Bergh had indicated that PSO does not guarantee the convergence to the global optimum. Particularly, when the dimensions of objective functions are high and numerous local optima coexist, PSO is easily trapped into local optima resulting in a low optimizing precision or even failure. When this occurs, simply enlarging the population size or increasing the evolution run-times will not facilitate improving the optimizing performance [27–30].

In this research work, an effort is made to optimize the tribological and mechanical properties of diffusion alloyed Fe-Ni-Cu steel powders. PSO was used to sweep a region of interest and select the optimal settings to a process. The PSO is a global optimization algorithm, and the objective function does not need to be differentiable. This allows the algorithm to be used in solving difficult problems, such as multimodals. Many researchers have worked on this problem and proposed many improved versions of PSO. For example, van den Bergh proposed a cooperative particle swarm optimizer and further combined it with PSO in an attempt to achieve the best properties of both algorithms [28–32]. Liang proposed a dynamic multiswarm particle swarm optimizer which showed a better performance in CEC2006, and subsequently Zhao further improved it for large scale optimization with a Quasi-Newton local search in CEC2008. Huang et al. proposed a comprehensive learning particle swarm optimizer, which uses a novel learning strategy, where all other particle's best historical information is used to update a particle's velocity. This strategy enables the diversity of the swarm to be preserved to discourage premature convergence. Kennedy [30] proposed the fully informed particle swarm and the simulation results showed that it was a promising method for benchmark functions [27–31]. While there are a lot of PSO variants as mentioned above, the optimizing results for some problems are still unacceptable. Since there is not any published work regarding estimation and prediction of wear behavior of sintered steels using PSO, this paper focuses on development of these models. The PSO is further improved in this work.

Table 1. Composition of the powders

Element	C	Cu	Ni	Mo
wt.%	> 0.01	1.5	4	0.5

Table 2. Size analysis of the powders

Powders Mesh Analysis	
+212 μm	0 %
+150 μm	7 %
–50 μm	25 %

2. Experimentals

In this study, partially alloyed powders were selected for the experiment. The Fe-Ni-Cu steel alloy has proven to meet demand for high performance parts in a cost efficient way. Strong impact for development of the new application has been achieved. The composition, size analysis and properties of the used powders are presented in Tables 1, 2 and 3, respectively. Carbon (0.6 wt.%) as fine natural graphite (UF4) and zinc stearate (0.75 wt.%) as lubricant were added to the mixture. Table 4 shows the characteristics of the graphite used in the mixture.

The samples were compacted with different pressures using a hydraulic machine (100 tons capacity)

Table 3. Properties of the powders

Compressibility at 600 MPa	Apparent density	Hydrogen loss	Flowability
7.15 ($g\,cm^{-3}$)	4.00 ($g\,cm^{-3}$)	0.10 %	26 (s/50g)

Table 4. Characteristics of the graphite used in the mixture

Type	Density (g cm^{-3})	Element (ppm)				
		Fe	Cu	Mg	Al	Si
UF4	1.859	551	87	130	253	604

at 120 ℃. The compacted samples were sintered at 1120 ℃ for 30 min in 90 % N_2/10 % H_2 atmosphere. The sintered densities of samples were measured in accordance with ASTM-B328 standard. Table 5 represents the effect of the applied pressure on the density and porosity of the studied materials.

The mechanical properties including tensile strength and hardness were carried out according to ASTM E8-00 and ASTM E92-82 standards, respectively. The hardness test method covers the determination of the Vickers hardness of materials, using applied force of 10 kgf. Each value of hardness and tensile strength is an average of at least three tests.

Dry sliding wear tests were performed under different loads of 10, 20, 30, 40 and 60 N using a pin-on-disc type reciprocate wear apparatus.

The samples were put in contact with AISI 52100 steel pins with 64 HRC. Table 6 shows the chemical composition of AISI 52100 steel.

All tests were performed at room temperature (21 ℃, relative humidity 30–60 %). Total sliding distance was selected as 2000 m.

For microstructure study, specimens were prepared by grinding through 120, 400, 600, 800 grit papers followed by polishing with 9 µm diamond paste and etched with 3 % nital solution. A set of three samples was tested in every experimental condition, and the average along with standard deviation for each set of three tests is measured.

3. TV-MOPSO

This section describes the proposed PSO approach to multi-objective optimization (MOO) problem. The motivation behind this concept is to attain better convergence to the Pareto-optimal front, while giving sufficient emphasis to the diversity consideration. In TV--MOPSO, a new parameter has been incorporated that ensures the diversity of the solutions in the archive [25–32].

Table 6. Chemical composition of AISI 52100 steel

Element	Fe	Cr	Mn	Si	C	S
wt.%	balance	1.5	0.35	0.2	1.1	0.025

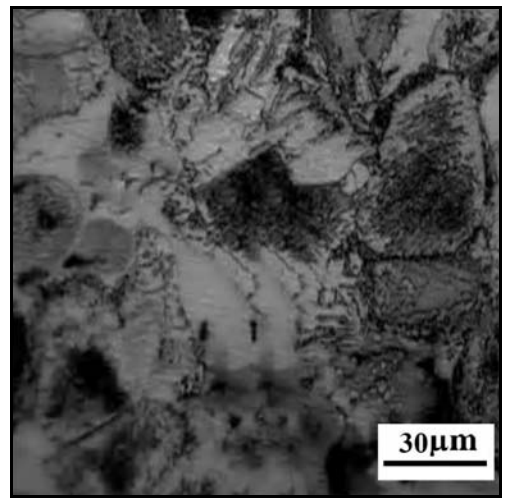

Fig. 1. Typical microstructure of the studied materials.

4. Results and discussion

Typical microstructure of the studied sample is presented in Fig. 1. It is noted that various phases form the microstructure of the porous samples including the ferrite and perlite. Figure 2 shows optical micrographs of the samples with different porosity levels depending on the applied pressure during cold pressing. The homogenous distributed porosity in these samples is the combination of the pores that are present among the compacted powders and not removed by pressing as an intrinsic feature of powder metallurgy products and also residual porosity from

Table 5. The influence of the applied pressure on the density of the porous steel fabricated in this study

Type of sample	PM_1	PM_2	PM_3	PM_4	PM_5	PM_6	PM_7	PM_8	PM_9	PM_{10}
Applied pressure (MPa)	300	350	400	450	500	550	600	650	700	750
Density (g cm^{-3})	6.83	6.87	6.93	6.98	7.03	7.07	7.12	7.19	7.32	7.44
Porosity (vol.%)	17.4	15.8	14.9	14.1	13.6	12.7	12.2	11.3	10.5	9.2

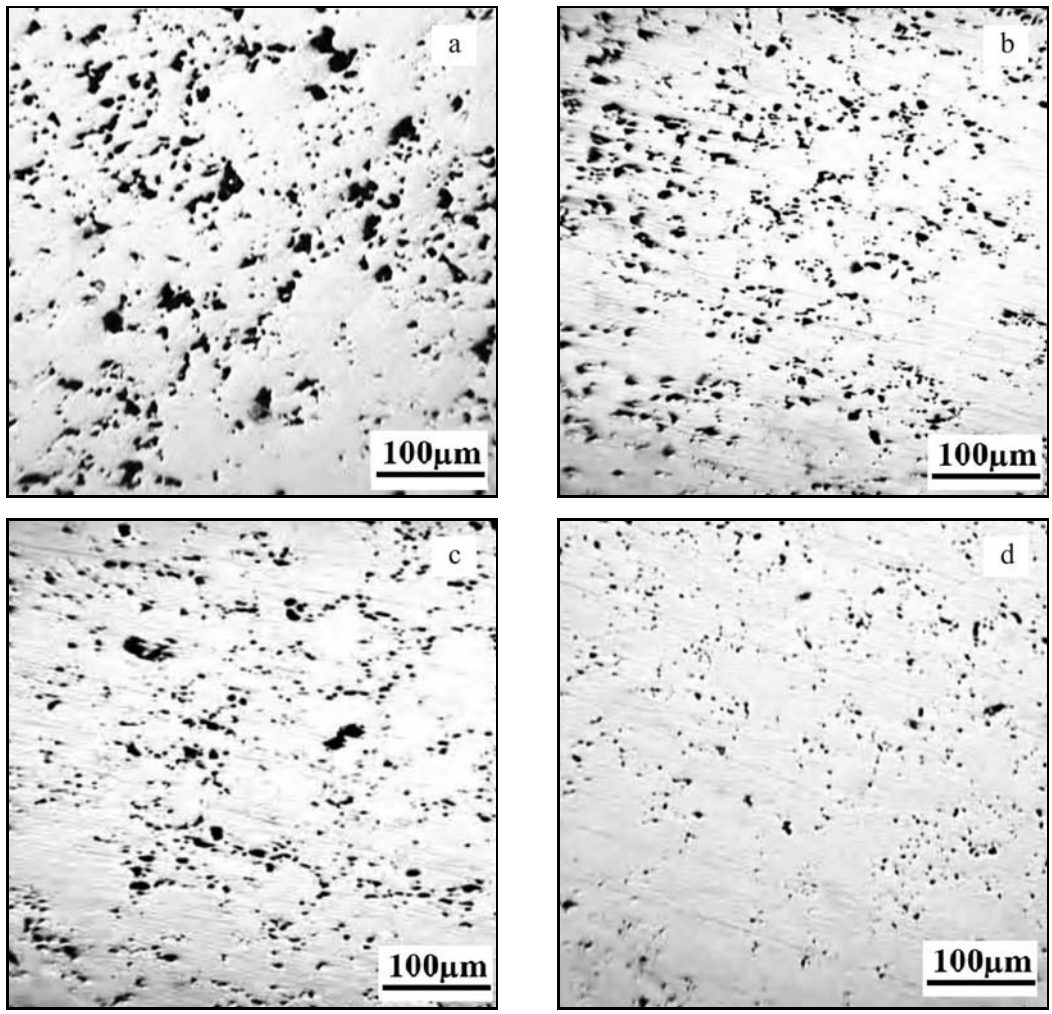

Fig. 2. Optical micrographs of the samples: (a) PM_1, (b) PM_4, (c) PM_6, (d) PM_{10}.

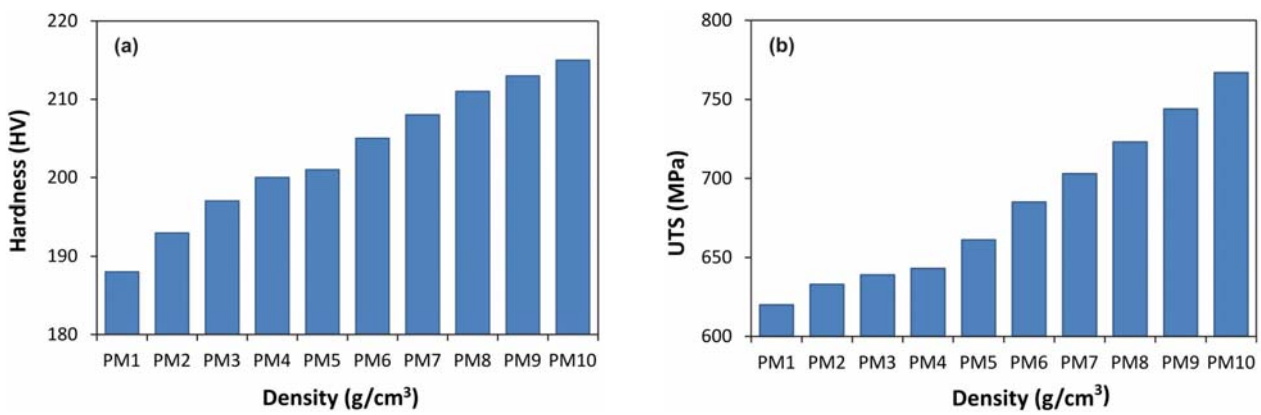

Fig. 3. Mechanical properties of studied materials: (a) HRB, (b) UTS.

liquid phase formation or diffusion of alloying additions, such as copper, at the sintering temperature. In PM materials, there are several microstructural parameters, e.g., pore-related parameters, to be taken into account, which are relevant for mechanical and tribological behavior. The hardness test was carried out for each sample. Ten hardness readings on randomly selected regions were taken in order to get a representative value of hardness. During hardness measurement, precaution was taken to make indentation at a distance of at least twice the diagonal length of the previous indention. Figure 3a shows that the hardness

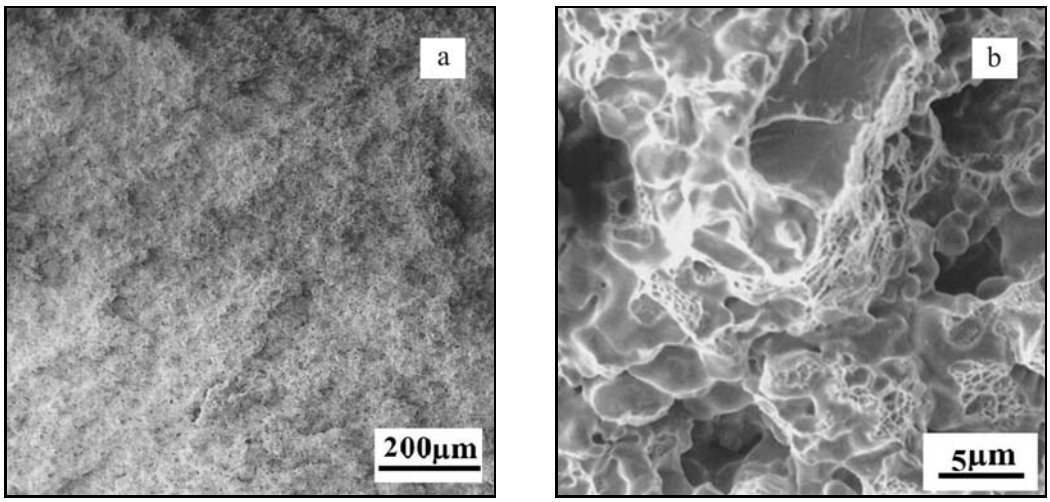

Fig. 4. SEM micrographs of tensile fracture surfaces: (a) low magnification, (b) high magnification.

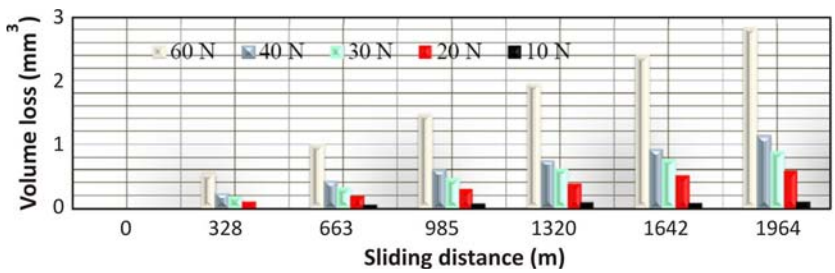

Fig. 5. The variations of volume loss with the sliding distance for PM_2 samples under different loads.

of samples increases with decreasing amount of porosity. It is clearly shown that the hardness takes into account the porosity content of the materials. Figure 3b shows the variations of UTS with the porosity content. It indicates that increasing amount of UTS is observed with increasing the density. It has been reported in previous research that the presence of pores causes reductions in strength and ductility [17–19]. The crack initiation takes place at the preferred site like pores, particularly at the surface of the specimen. Thus, more crack nucleation occurs in the samples with lower density. Then these cracks connect together in all volume of sample and have a destructive effect on the tensile strength and hardness of the materials [3, 20–15]. Typical SEM micrographs of tensile fracture surfaces are shown in Fig. 4. Fracture surface observations of the samples show the contribution of both fracture mechanisms. Some areas of the fracture surfaces consist of dimples which may be a result of the void nucleation and subsequent coalescence by strong shear deformation and fracture process on the shear plane.

The typical variations of volume loss with sliding distance for the PM_2 samples are summarized in Fig. 5. It is clear from this graph that the volume loss increases with increasing the applied load. The effective wear from the specimen surface is due to the combined effect of a number of factors. The increase in the applied load leads to increase in the penetration of hard asperities of the counter surface to the specimen surface, increase in micro cracking tendency of the subsurface and also increase in the deformation and fracture of asperities of the softer surface. On the other hand, higher amount of material from the specimen surface gets accumulated at the valleys between the asperities of counter surfaces resulting in reduction in height and cutting efficiency of counter surface asperities.

The load at which wear rate increases suddenly to a very high value is termed as the transition load. When the applied load is greater than the transition load, the wear rate shoots up to a significantly higher value.

This is attributed to the significantly higher frictional heating, and thus the localized adhesion of the sample surface with the counter surface and also an increase in softening of the surface material, and thus more penetration of the asperities. Under such conditions the material removal due to the delamination of adhered areas, micro cutting and micro fracturing increase significantly. During the sliding, in fact, a considerable fraction of energy is spent on overcoming the frictional force, which leads to heating of the contact surfaces. Thus, it is expected that initially the tem-

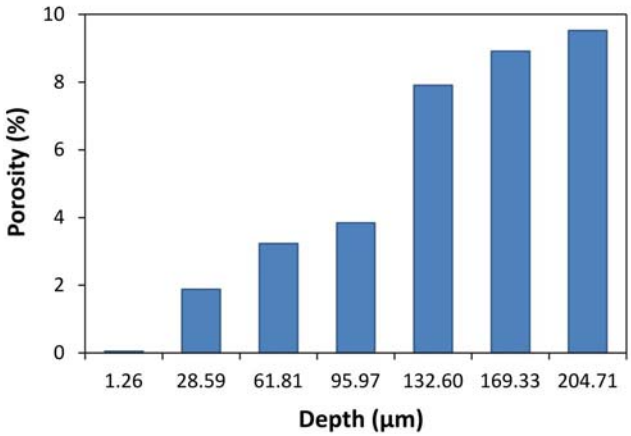

Fig. 6. The pores profile of the worn surface.

perature of the contact surface is less, and hence the asperities are expected to be stronger and more rigid. As time progresses, the frictional heating increases, which leads to higher temperature and softening of the surface materials.

The investigation of the worn surfaces revealed that various mechanisms including surface plastic deformation, oxidation and abrasion wear were involved in the wear of the materials. In general, a worn surface may have parallel and vertical forces acting on it which are the results of frictional stress and normal pressure of the abrasive pins [11, 12]. These forces cause an intensive shear stress on surface and sub surface layers.

In the initialization phase of TV-MOPSO, the swarm of size *Ns* is randomly generated. The individuals of the swarm are assigned random values for the coordinates, from the respective domains, for each dimension. Similarly the velocity is initialized to zero in each dimension. Initial value for the parameter Personal Best Performance (p_{best}) is set to X_i, where X_i is the ith particle [30]. The update step of TV-MOPSO deals with the simulation of the flight of the particles. Movement of a particle in the search space is mainly governed by its individual experience and by the experience of the group, with which it interacts directly [27–32].

In porous sintered samples, the plastic deformation results in pores closing and hardening of the surface layers. The pores content of the worn surface (PM_3) is shown in Fig. 6. As anticipated, decreasing amount of porosity is observed in the layers close to the surface. Because of combined action of load, sliding speed and sliding distance, subsurface micro cracks are generated which finally leads to removal of wear debris, especially from asperity contacts. In addition, higher temperature rise also leads to greater flowability of surface materials, and thus increases greatly the possibility of compaction of wear debris on the specimen surface [8–10].

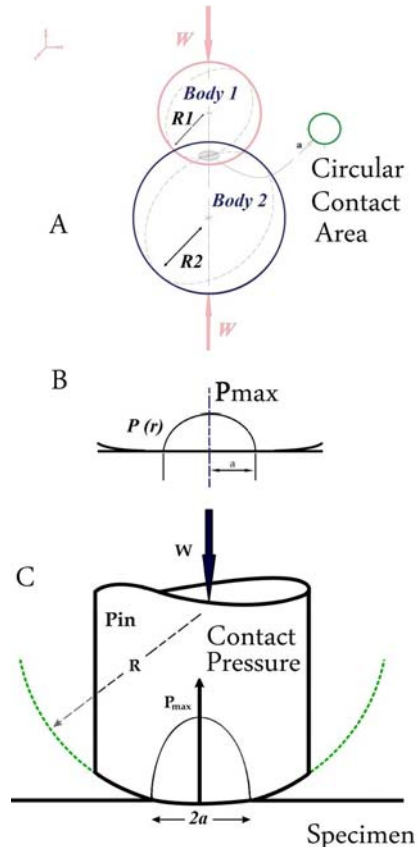

Fig. 7. (a) Elastic contact between two spheres under the load of *W*, (b) the stress distribution in the contact area of two spheres, (c) elastic contact between pin and samples.

In order to model the surface and subsurface mechanical stress, Hertz and Hamilton equations are utilized [33–35]. Figure 7a shows elastic contact between two spheres under the load of *W*. Hertz showed that the radius of circular contact surface between these two spheres can be obtained by:

$$a = \left(\frac{3WR}{4E}\right)^{1/3}, \tag{1}$$

where R is reduced radius of curvature and is obtained by Eq. (2). The equivalent elastic module, E, depends on the elastic modules of both spheres and is calculated by Eq. (3).

$$\frac{1}{R} = \frac{1}{R_1} + \frac{1}{R_2}, \tag{2}$$

$$\frac{1}{E} = \frac{(1-\upsilon_1^2)}{E_1} + \frac{(1-\upsilon_2^2)}{E_2}. \tag{3}$$

The stress distribution in the contact area, $P(r)$, and elastic contact between pin and sample are shown

in Fig. 7b and c, respectively. The stress distribution is defined as a function of maximum stress $P_{\max}$ which acts on the middle of contact surface.

$$P(r) = P_{\max}\sqrt{\left(1-\frac{r^2}{a^2}\right)},\ r^2 = x^2+y^2. \quad (4)$$

The presence of friction inevitably affects the stress distribution in each point of the surface:

$$Q(r) = \mu P(r). \quad (5)$$

Thus, the stress distribution on the surface:

$$Q(r) = \mu P(r) = \mu p_{\max}\sqrt{\left(1-\frac{r^2}{a^2}\right)} = \\ = \frac{3\mu w}{2\pi a^2}\sqrt{\left(1-\frac{r^2}{a^2}\right)}. \quad (6)$$

Friction coefficient measurement is carried out, and mean friction coefficient (μ) is 0.7. Also, subsurface stress can be obtained by:

$$\sigma_x = \frac{3Q}{2\pi a^3}\left[-x\left(\frac{\upsilon}{4}+1\right)\phi + \frac{axM}{r^4}\cdot\right. \\ \cdot\left\{\left(\frac{3}{2}-\frac{2x^2}{r^2}\right)\left(S\upsilon-2A\upsilon+z^2\right)+\frac{x^2z^2}{3}+\right. \\ +\frac{7\upsilon r^2}{4}-2\upsilon x^2+r^2\Bigg\}+ \\ +\frac{xzN}{r^4}\left\{\left(\frac{3}{2}-\frac{2x^2}{r^2}\right)\left[-\frac{S}{6}(1-2\upsilon)-\frac{A}{3}(1-2\upsilon)-\right.\right. \\ \left.-\frac{1}{2}(z^2+3a^2)\right]+\frac{a^2x^2}{S}-\frac{\upsilon r^2}{4}-\frac{7r^2}{4}\Bigg\}+ \\ \left.+\frac{4a^3xz}{3r^4}\left(\frac{3}{2}-\frac{2x^2}{r^2}\right)(1-2\upsilon)\right], \quad (7)$$

$$\sigma_y = \frac{3Q}{2\pi a^3}\left[-\frac{3\upsilon x\phi}{4}+\frac{axM}{r^4}\left\{\left(\frac{1}{2}-\frac{2y^2}{r^2}\right)\cdot\right.\right. \\ \cdot\left(S\upsilon-2A\upsilon+\upsilon r^2+z^2\right)+\frac{y^2z^2}{S}+\frac{3\upsilon r^2}{4}\Bigg\}+ \\ +\frac{xzN}{r^4}\left\{\left(\frac{1}{2}-\frac{2y^2}{r^2}\right)\left[-\frac{S}{6}(1-2\upsilon)-\frac{A}{3}(1-2\upsilon)-\right.\right. \\ \left.-\frac{1}{2}(z^2+3a^2)\right]+\frac{a^2y^2}{S}-\frac{3\upsilon r^2}{4}-\frac{r^2}{4}\Bigg\}+ \\ \left.+\frac{4a^3xz}{3r^4}\left(\frac{1}{2}-\frac{2y^2}{r^2}\right)(1-2\upsilon)\right], \quad (8)$$

$$\sigma_z = \frac{3Q}{2\pi a^3}\left[\frac{xzN}{2r^2}\left\{1-\frac{z^2+a^2+r^2}{S}\right\}\right], \quad (9)$$

$$\tau_{xy} = \frac{3Q}{2\pi a^3}\left[\frac{y}{2}\left(\frac{\upsilon}{2}-1\right)\phi+\frac{ayM}{r^4}\cdot\right. \\ \cdot\left\{\frac{x^2z^2}{S}+\upsilon\left[(S-2A)\left(\frac{1}{2}-\frac{2x^2}{r^2}\right)-2x^2+\frac{r^2}{4}\right]+\right. \\ +\frac{r^2}{2}+z^2\left(\frac{1}{2}-\frac{2x^2}{r^2}\right)\Bigg\}+\frac{yzN}{r^4}\Bigg\{\left(\frac{1}{2}-\frac{2x^2}{r^2}\right)\cdot \\ \cdot\left[(2\upsilon-1)\left(\frac{S}{6}+\frac{A}{3}\right)-\frac{1}{2}\left(z^2+3a^2+r^2\right)\right]+ \\ +\frac{r^2\upsilon}{4}+\frac{a^2x^2}{S}-\frac{y^2}{2}-\frac{3x^2}{2}\Bigg\}+ \\ \left.+\frac{4a^3yz}{3r^4}\left(\frac{1}{2}-\frac{2x^2}{r^2}\right)(1-2\upsilon)\right], \quad (10)$$

$$\tau_{yz} = \frac{3Q}{2\pi a^3}\frac{xyz}{2r^4}\left[aM\left\{\frac{1}{2}+\frac{1}{2S}(z^2-3a^2-r^2)\right\}+\right. \\ \left.+\frac{zN}{2}\left\{-3+\frac{1}{S}(5a^2+z^2+r^2)\right\}\right], \quad (11)$$

$$\tau_{zx} = \frac{3Q}{2\pi a^3}\left[\frac{3z\phi}{2}+\frac{azM}{r^2}\left\{1+\frac{x^2}{r^2}-\frac{x^2}{S}\right\}+\right. \\ +\frac{N}{r^2}\Bigg\{-\frac{3}{4}(S+2A)+z^2-\frac{3}{4}a^2- \\ \left.-\frac{1}{4}r^2+\frac{z^2}{2}\left(\frac{1}{2}-\frac{2x^2}{r^2}\right)\Bigg\}\right], \quad (12)$$

where A, S, M, N, G and H are defined as: $A = r^2+z^2-a^2$, $S = \sqrt{A^2+4a^2z^2}$, $r^2 = x^2+y^2$, $M = \sqrt{\frac{S+A}{2}}$, $N = \sqrt{\frac{S-A}{2}}$, $\phi = \arctan\left(\frac{a}{M}\right)$, $G = M^2-N^2+zM-aN$, $H = 2MN+aM+zN$.

Figure 8 displays the stress distribution on the worn surface and subsurface. It is observed that the plastic deformation and decrease in porosity percentage occur in the layers where equivalent effective stress is higher than tensile stress.

In PSO, the individual experience of the particle is captured in the p_{best} attribute that corresponds to the best performance attained so far by it in its flight.

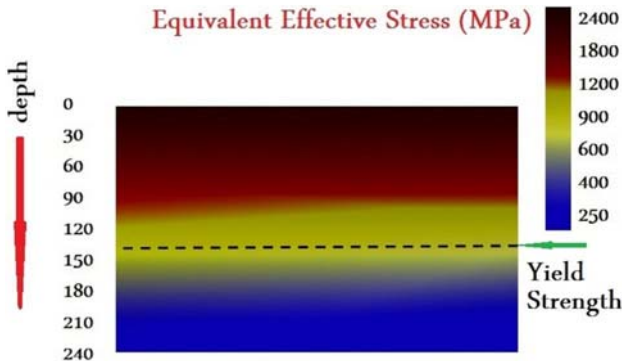

Fig. 8. Stress distribution on the worn surface.

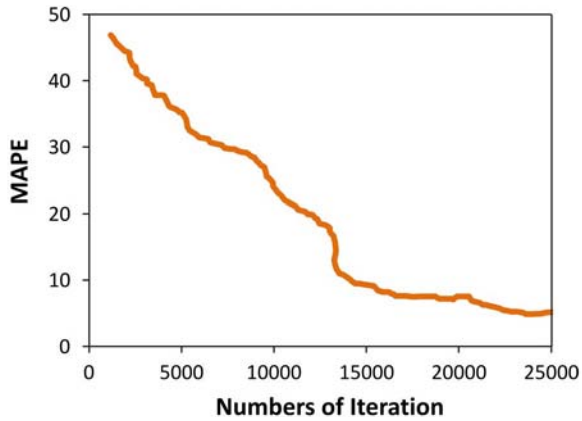

Fig. 9. The effect of iteration number on the MAPE.

In TV-MOPSO, the present solution is compared with the p_{best} solution, and it replaces the latter only if it dominates that solution.

The term g_{best} (Global Best Performance) represents the best solution obtained by the swarm [30]. Often the conflicting nature of the multiple objectives involved in MOO problems makes the choice of a single optimum solution difficult. To resolve this problem, the concept of non-dominance is used and an archive of non-dominated solutions is maintained, from which a solution is picked up as the g_{best}. TV-MOPSO maintains an archive that has its maximum size limit. The selection of the g_{best} solution is done from the archive on the basis of the diversity of the solutions as in [30].

In order to improve the convergence of PSO, a strategy for the incorporation of inertia weight w is suggested. The parameter w controls the influence of the previous velocity on the present velocity.

The higher values of w help in the global search for the optimal solution, while lower values help in the local search around the current search area. All the population based search techniques rely on global exploration and local exploitation in order to achieve good performance [30]. Generally, more exploration should be carried out in the initial stages when the algorithm has very little knowledge about the search space. In contrast, more exploitation is needed in the later stages so that the algorithm is able to exploit the information it has gained so far. The movement of the particle towards the optimum solution is governed by updating its position and velocity attributes. The velocity and position update equations are given as:

$$V_{i,j} = wV_{i,j} + c_1 r_1 (P_{i,j} - X_{i,j}) + c_2 r_2 (P_{g,i} - X_{i,j}), \quad (13)$$

where $j = 1, \ldots, d$ and w, c_1, $c_2 \geq 0$, w is the inertia weight, c_1 and c_2 are the acceleration coefficients, and r_1 and r_2 are random numbers, generated uniformly in the range [0, 1], responsible for providing randomness to the flight of the swarm [30]. The term $c_1 r_1 (P_{i,j} - X_{i,j})$ in Eq. (13) is called cognition term, whereas the term $c_2 r_2 (P_{g,j} - X_{i,j})$ is called the social term. The cognition term takes into account only the particle's individual experience, whereas the social term signifies the interaction between the particles. The c_1 and c_2 values allow the particle to tune the cognition and the social terms, respectively, in the velocity update equation. A larger value of c_1 allows exploration, while a larger value of c_2 encourages exploitation [25–29]. Since the selection of the g_{best} solution is done from the archive in TV-MOPSO, it plays a very vital role. At each iteration, the archive gets updated with the inclusion of the non-dominated solutions from the combined population of the swarm and the archive.

The single objective PSO algorithms have been found to show good convergence properties. However, for the multi-objective PSOs, this convergence is usually achieved at the cost of the diversity. To allow the multi-objective PSO algorithm to explore the search space to a greater extent, while obtaining better diversity, a mutation operator has been used in TV--MOPSO, that is based on the one found in. Similar mutation operator has been used in PSO for multi--modal function optimization.

The algorithm terminates after executing a specified number of iterations. After termination, the archive contains the final non-dominated front.

Figure 9 shows the effect of iteration number on the MAPE of developed model. The number of iteration was selected to be 25000. Inertia weight w linearly decreased from 0.9 to 0.4; the learning rates were $c_1 = c_2 = 2$; $V_{\min}$ was equal to $X_{\min}$; $V_{\max}$ equal to $X_{\max}$. Final optimized parameters are 432.63 MPa applied pressure, 6.962 g cm^{-3} density, 14.41 % porosity, 2.81 mm^3 volume loss, 641.75 MPa UTS and 201.56 BHN hardness. The results show that the novel technique implemented in this investigation has an acceptable performance. Therefore, this work shows the usefulness of an intelligent way to predict the performance of wear behavior using TV-MOPSO.

5. Conclusion

In the present article, a novel multi-objective PSO algorithm, called TV-MOPSO, has been presented. TV-MOPSO is adaptive in nature with respect to its inertia weight and acceleration coefficients. This adaptiveness enables it to attain a good balance between the exploration and the exploitation of the search space. A mutation operator has been incorporated in TV-MOPSO to resolve the problem of premature convergence to the local Pareto-optimal front. Experimental observation indicated that the main wear mechanisms were oxidation wear and surface plastic deformation caused by metallic particle detachment, as well as abrasion wear resulted from abrasive debris agglomeration. Meanwhile, variation of dry sliding wear resistance of this alloy with porosity shows that the porosity is beneficial for wear resistance when wear debris is entrapped and formation of large abrasive agglomerates is prevented. But conditions of wear tests such as applied load also have significant effect on this behavior, and with applying various loads, the role of porosity in wear behavior will change. The increasing amounts of UTS and hardness are observed with increasing the density.

References

[1] Shabani, M. O., Mazahery, A.: Ceramics Int., *38*, 2012, p. 4541. doi:10.1016/j.ceramint.2012.02.031

[2] Shabani, M. O., Mazahery, A.: Powder Technol., *217*, 2012, p. 558. doi:10.1016/j.powtec.2011.11.020

[3] Shabani, M. O., Mazahery, A.: JOM, *64*, 2012, p. 323. doi:10.1007/s11837-012-0245-0

[4] Sarasola, M., Gomez-Acebo, T., Castro, F.: Acta Mater., *52*, 2004, p. 4615. doi:10.1016/j.actamat.2004.06.018

[5] Suh, N. P.: Wear, *44*, 1977, p. 1. doi:10.1016/0043-1648(77)90081-3

[6] Sudhakar, K. V., Sampathkumaran, P., Dwarakadasa, E. S.: Wear, *242*, 2000, p. 207. doi:10.1016/S0043-1648(00)00422-1

[7] Molinari, A., Straffelini, G.: Wear, *173*, 1994, p. 121. doi:10.1016/0043-1648(94)90264-X

[8] Lim, S. C., Brunton, J. H.: Wear, *113*, 1986, p. 371. doi:10.1016/0043-1648(86)90035-9

[9] Leheup, E. R., Zhang, D., Moon, J. R.: Wear, *221*, 1998, p. 86. doi:10.1016/S0043-1648(98)00265-8

[10] Straffellini, G., Molinari, A.: Powder Metall., *44*, 2001, p. 248. doi:10.1179/003258901666419

[11] Simchi, A., Danninger, H.: Powder Metall., *47*, 2004, p. 73. doi:10.1179/003258904225015545

[12] Molinari, A., Straffelini, G., Campestrini, P.: Powder Metall., *42*, 1999, p. 235. doi:10.1179/003258999665576

[13] Gulsoy, H. O.: Scr. Mater., *52*, 2005, p. 187. doi:10.1016/j.scriptamat.2004.09.032

[14] Gulsoy, H. O., Bilici, M. K.: Mater & Design, *28*, 2007, p. 2255. doi:10.1016/j.matdes.2006.05.022

[15] Mazahery, A., Shabani, M. O.: Trans. Nonferrous Met. Soc. China, *22*, 2012, p. 275. doi:10.1016/S1003-6326(11)61171-0

[16] Dubrujeaud, B., Vardavoulias, M.: Wear, *174*, 1994, p. 155. doi:10.1016/0043-1648(94)90097-3

[17] Mathew, B. A., Mastromatteo, R.: Metal Powder Report, *57*, 2002, p. 20. doi:10.1016/S0026-0657(02)85078-0

[18] Bocchini, G. F.: International Journal of Powder Metallurgy, *22*, 1986, p. 185.

[19] Klar, E., Samal, P. K.: In: ASM Handbook, Powder Metal Technologies and Applications. Vol. 7. ASM International, OH 1994. PMid:11271188

[20] Hadrboletz, A., Weiss, B.: Int. Mater. Rev., *42*, 1997, p. 44. doi:10.1179/095066097790326029

[21] Mazahery, A., Shabani, M. O.: Powder Technol., *225*, 2012, p. 101. doi:10.1016/j.powtec.2012.03.039

[22] Sadigh, A. N., Mozafari, M., Karimi, B.: Advances in Engineering Software, *45*, 2012, p. 144. doi:10.1016/j.advengsoft.2011.09.008

[23] Mazahery, A., Shabani, M. O.: Composites: Part B, *43*, 2012, p. 1302. doi:10.1016/j.compositesb.2012.01.011

[24] Shabani, M. O., Mazahery, A.: Trans Indian Inst Met, *65*, 2012, p. 77. doi:10.1007/s12666-011-0110-9

[25] Shabani, M. O., Mazahery, A., Bahmani, A., Davami, P., Varahram, N.: Kovove Mater., *49*, 2011, p. 253. doi:10.4149/km_2011_4_253

[26] Pendharkar, P. C.: Computers & Operations Research, *32*, 2005, p. 2561. doi:10.1016/j.cor.2004.06.023

[27] Shabani, M. O., Mazahery, A.: Synth. Metal., *161*, 2011, p. 1226. doi:10.1016/j.synthmet.2011.04.009

[28] Yoshida, H., Kawata, K., Fukuyama, Y.: IEEE Transactions on Power Systems, *15*, 2000, p. 1232. doi:10.1109/59.898095

[29] Shabani, M. O., Mazahery, A.: Appl. Math. Model., *35*, 2011, p. 5707. doi:10.1016/j.apm.2011.05.008

[30] Shabani, M. O., Mazahery, A.: Appl. Math. Model., *36*, 2011, p. 5455. doi:10.1016/j.apm.2011.12.059

[31] Shabani, M. O., Mazahery, A., Rahimpour, M. R., Tofigh, A. A., Razavi, M.: Kovove Mater., *50*, 2012, p. 25. doi:10.4149/km_2012_1_25

[32] Shabani, M. O., Mazahery, A.: Metall. Mater. Trans. A, *43*, 2012, p. 2158. doi:10.1007/s11661-011-1040-1

[33] Hamrock, B. J., Dowson, D.: Ball Bearing Lubrication. John Wiley & Sons Publication 1981.

[34] Hamilton, G. M., Goodman, L. E.: ASME, J Appl. Mech., *88*, 1966, p. 371. doi:10.1115/1.3625051

[35] Mazahery, A., Shabani, M. O., Rahimpour, M. R., Tofigh, A., Razavi, A.: Kovove Mater., *50*, 2012, p. 107. doi:10.4149/km_2012_2_107